A new integrated approach to cardiac mechanics: reference values for normal left ventricle

Giorgio Faganello[1] · Dario Collia[2] · Stefano Furlotti[1] · Linda Pagura[1] · Michele Zaccari[1] · Gianni Pedrizzetti[2] · Andrea Di Lenarda[1]

Accepted: 3 July 2020

Abstract

The association between left ventricular (LV) myocardial deformation and hemodynamic forces is still mostly unexplored. The normative values and the effects of demographic and technical factors on hemodynamic forces are not known. The authors studied the association between LV myocardial deformation and hemodynamic forces in a large cohort of healthy volunteers. One-hundred seventy-six consecutive subjects (age range, 16–82; 51% women), with no cardiovascular risk factors or any relevant diseases, were enrolled. All subjects underwent an echo-Doppler examination. Both 2D global myocardial and endocardial longitudinal strain (GLS), circumferential strain (GCS), and the hemodynamic forces were measured with new software that enabled to calculate all these values and parameters from the three apical views. Higher LV mass index and larger LV volumes were found in males compared to females (85 ± 17 vs 74 ± 15 g/m^2 and 127 ± 28 vs 85 ± 18 ml, $p < 0.0001$ respectively) while no differences of the mean values of endocardial and myocardial GLS and of myocardial GCS were found ($p = ns$) and higher endocardial GCS in women (-30.6 ± 4.2 vs -31.8 ± 3.7; $p = 0.05$). LV longitudinal force, LV systolic longitudinal force and LV impulse were higher in men (16.2 ± 5.3 vs 13.2 ± 3.6; 25.1 ± 7.9 vs 19.4 ± 5.6 and 20.4 ± 7 vs 16.6 ± 5.2, $p < 0.0001$, respectively). A weak but statistically significant decline with age ($p < 0.0001$) was also found for these force parameters. This new integrated approach could differentiate normality from pathology by providing average deformation values and hemodynamic forces parameters, differentiated by age and gender.

Keywords Cardiac mechanics · Hemodynamic forces · Deformation imaging · Echocardiography

Introduction

The non-invasive and correct calculation of the left ventricle ejection fraction (LVEF) represents an essential challenge in modern cardiology. Although LVEF is the most often used parameter to evaluate the LV function and is associated with adverse cardiovascular outcomes [1], LVEF is not sufficiently sensitive to detect subtle myocardial dysfunction [2]. Strain imaging has a higher prognostic value to conventional measures for predicting major adverse cardiac events [3]. We recently provided a mathematical relationship showing that the LVEF can be expressed in terms of global longitudinal strain (GLS) and global circumferential strain (GCS); the combined use of the LVEF and the strain imaging represents a promising tool in the hands of clinicians [4]. Besides, a relatively new imaging marker of LV function such as longitudinal (base-apex oriented) hemodynamic forces, or equivalently intraventricular pressure gradients (IVPGs), represents further progress in myocardial deformation imaging

✉ Giorgio Faganello
giorgio.faganello@asugi.sanita.fvg.it

Dario Collia
dar.collia@gmail.com

Stefano Furlotti
s.furlotti@gmail.com

Linda Pagura
lindapagura91@gmail.com

Michele Zaccari
mzaccari00@gmail.com

Gianni Pedrizzetti
giannip@dia.units.it

Andrea Di Lenarda
andrea.dilenarda@asugi.sanita.fvg.it

[1] Cardiovascular Department, Azienda Sanitaria Universitaria Giuliano Isontina, via Slataper n°9, 34100 Trieste, Italy

[2] Department of Engineering and Architecture, University of Trieste, P.le Europa 1, 34127 Trieste, Italy

in addition to the traditional parameters of volume [5–7]. Echocardiography-based hemodynamic forces assessment is still mostly unexplored [8] and requires reference values validation in the healthy population, but its use will allow a better understanding of the early alterations of cardiac mechanics with pathology. We designed this prospective study to establish normal reference limits for hemodynamic forces in healthy adults; to verify the relationships between the LV GLS and GCS with the LVEF and finally to examine the influence of age and sex on all these parameters.

Methods

Patient population

We prospectively enrolled 200 consecutive healthy subjects in a screening of cardiovascular prevention in the period between January and December 2019 and excluded 24 patients from the original study population, for poor-image quality. No subject had cardiovascular symptoms or risk factors (i.e., high blood pressure values, smoking, diabetes, and dyslipidemia). We applied as exclusion criteria histories of coronary artery disease, moderate/severe valvular heart diseases, congestive heart failure, congenital heart diseases, systemic diseases, pharmacological treatment, resting heart rhythm abnormalities, and all the patients under the age of 16. The study complies with the Declaration of Helsinki, and the Ethics Committee of the University of Trieste (protocol no. 0025052) approved the study. Written informed consent of all registered volunteers was obtained.

Standard 2D LV image acquisition and analysis

Standard echocardiography examinations were performed with Vivid E95 (GE Healthcare, Horten, Norway) machine equipped with a 2.5-MHz phased array transducer using a frame rate above 60, by a qualified professional following recommended protocols approved by the EACVI [9]. Three experienced operators, blinded to the clinical data, performed offline speckle-tracking (ST) and the LV quantitative analysis according to the 2015 ASE/EACVI recommendations [10]. The LV mass calculation was executed with linear measurements, using a formula validated by necropsy and normalized for body surface area [11, 12]. LV hypertrophy was defined as LV mass > 95 g/m^2 in women and > 115 g/m^2 in men [10]. Transmitral pulsed Doppler and pulsed tissue Doppler of septal mitral annulus were recorded in the apical 4-chamber view, and we determined the diastolic parameters and grades of LV diastolic dysfunction according to the current ASE/EACVI recommendations [13].

2D LV speckle tracking image analysis

The LV 2D strain was quantified using commercially available software (2DCPA v.1.3; TomTec Imaging Systems Gmbh, Unterschleissheim, Germany). We performed analyses in all three apical views (LV four-chambers, two-chambers, and three-chambers) and the most suitable cardiac cycle [8]. The software required to draw the end-systolic endocardial and epicardial borders and track them over the entire heartbeat; subsequently, it allowed us to correct the end-diastolic borders and to propagate the correction over the entire cardiac cycle without affecting the previously drawn end-systolic borders. Consequently, it was possible to obtain the end-systolic volume (ESV), the end-diastolic volume (EDV), and to measure the LVEF from the three-projections using the method of disks (modified Simpson's rule) according to the guidelines [14]. We calculated the longitudinal subendocardial strain by covering the endocardium with the border of the region of interest (ROI) and the transmural variation (myocardial strain) in the whole myocardium. From the same borders, we evaluated the LV diameters from base to apex, and their reduction from ED to ES, the average length of the LV, gave the GCS. The apical approach to GCS could have been less accurate because the entire circumference was not visible from the apical views; this criticality was minimized by using a triplane evaluation, thus applying the same approach and the same approximation commonly used in the evaluation of LV volumes. This approach to circumferential strain was more similar to the one used in 3D echocardiography because the border followed the tissue during its longitudinal motion and reduced artifacts in deformation such as those resulting from through-plane displacements of 3D geometry, that sometimes affect the short axis transversal projections [15]. From the same endocardial border obtained in the three apical views, we were able to calculate the LVEF. The operator could visually confirm the integrity of the automatic software detection and, if necessary, readjusted it (Fig. 1). Longitudinal and circumferential displacements, described by GLS and GCS, respectively, jointly contributed to the volumetric reduction and LVEF. A complex mathematical relationship between LVEF and myocardial strain [16] involving the diameters and average thicknesses of LV has been presented. This approach can be recast in more straightforward terms for endocardial strain values proving the explicit relationship [17]:

$$\mathrm{LVEF} = 1 - (\mathrm{GLS} + 1)\,(\mathrm{GCS} + 1)^2$$

This relationship will be used to analyze the results to demonstrate how the combined longitudinal and circumferential strains can lead to an LV volumetric reduction. The same ST data are then used to evaluate the hemodynamic forces

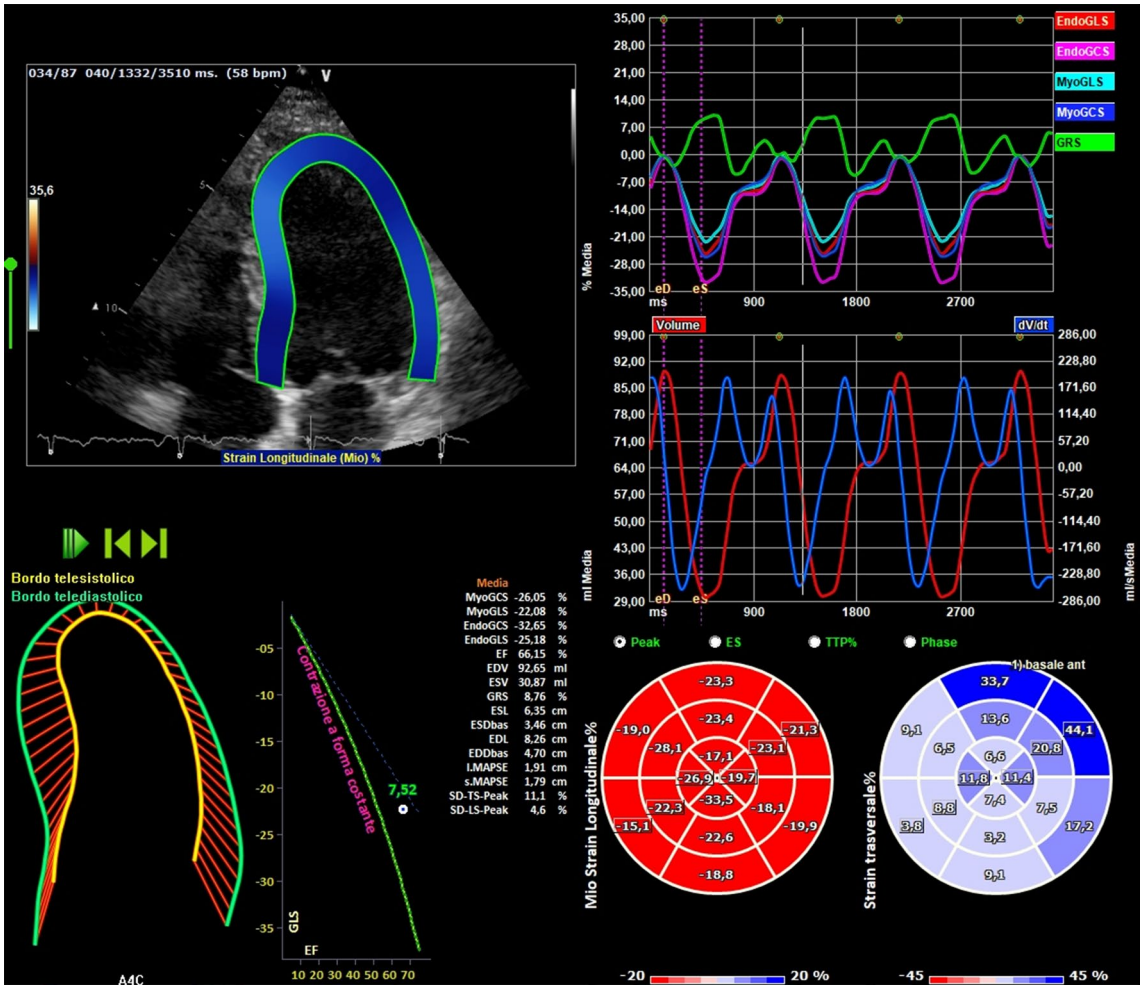

Fig. 1 Representative layer-specific speckle tracking analysis of longitudinal and circumferential strain

associated with blood flow (Fig. 2). We recently demonstrated how flow forces ("hemodynamic forces," "flow momentum" or "average IVPGs") could be detected through the knowledge of the LV geometry, endocardial velocities, obtained by ST, plus the area of the aortic and mitral orifices, carefully calculated by drawing the internal diameter of the valves annulus from the parasternal long axis-view [18]. The complete mathematical details of the method for transforming endocardial dynamics into flow forces are reported elsewhere, and the concept is only quickly summarized here [18]. The total hemodynamic force, $F(t)$, exchanged between blood and tissues can be computed by the balance of momentum inside the LV volume $V(t)$:

$$F(t) = \rho \int_{V(t)} \frac{\partial v}{\partial t} dV + \rho \int_{S(t)} v v_n dS;$$

where $S(t)$ is the surface bounding the volume, ρ is the fluid density, and $\boldsymbol{v}$ is the velocity vector where the subscript n indicates the normal outward component. The second term in the right-hand side of the previous formula represents the flux of momentum across the instantaneous LV volume boundary $S(t)$. The first term is blood inertia given by the rate of change of the velocity inside the LV volume. It can also be rewritten as the rate of velocity change across the boundaries so that the force can be computed from the information evaluated over the surface bounding the LV volume [19].

$$F(t) = \rho \int_{S(t)} x \frac{\partial v}{\partial t_n} dS + \rho \int_{S(t)} v v_n dS;$$

The longitudinal component of the hemodynamic force is obtained from the previous formula by introducing the longitudinal position for the position vector $\boldsymbol{x}$ in the first term, and the longitudinal velocity for the velocity vector $\boldsymbol{v}$ in the second term. The surface $S(t)$ bounding the LV volume is composed of a closed boundary, made of the endocardial surface, the closed part of the base, and an open boundary, given by the mitral and aortic valve, during diastole and

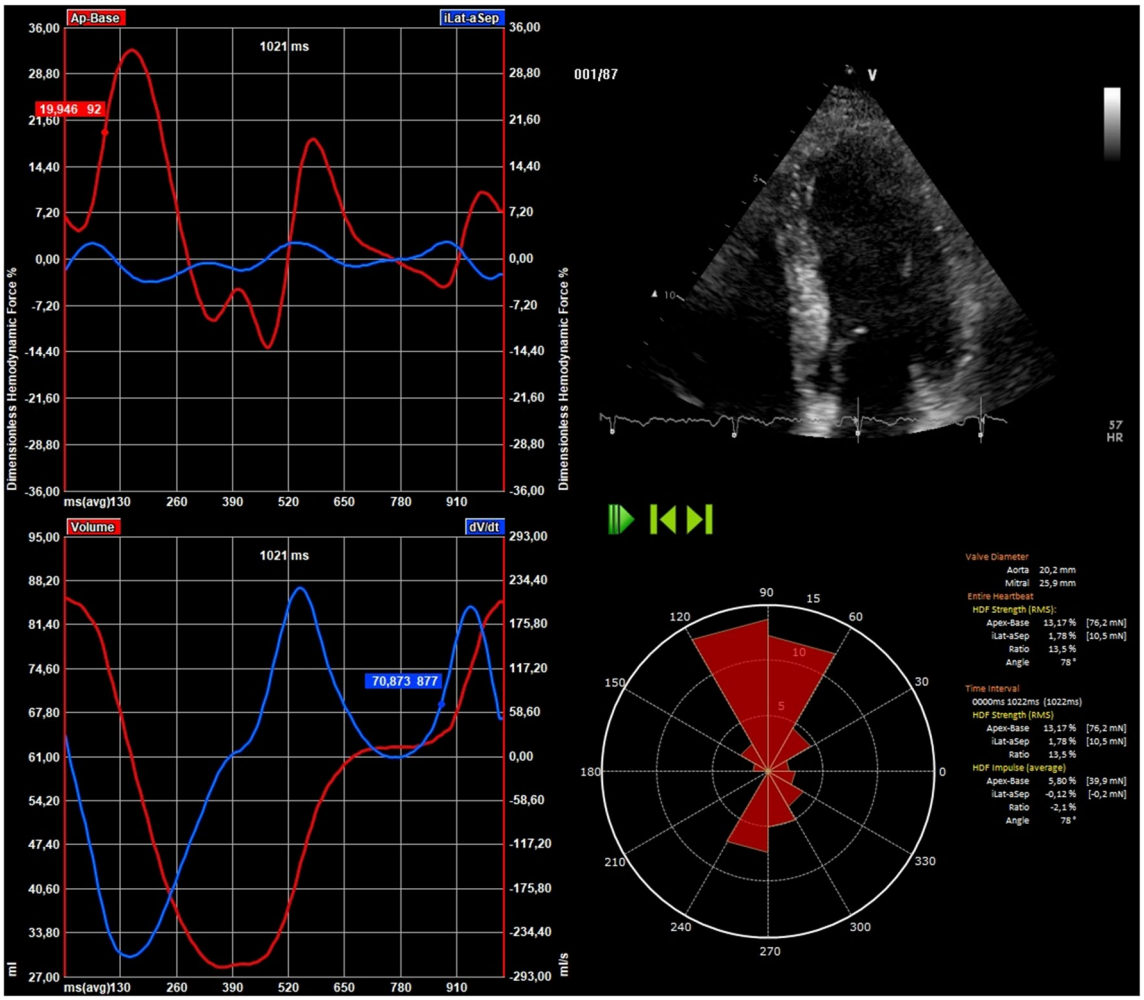

Fig. 2 Representative calculation of hemodynamic force parameters obtained by speckle tracking analysis

systole, respectively. The terms of the formula can thus be computed from the tissue velocity at the LV endocardium and at the base, which is known from ST, and from the mean velocity across the open valve, which is the LV volume rate divided by the valve area. The longitudinal hemodynamic forces will be used to analyze the results to integrate the volumetric and deformation information with those related to cardiac fluid dynamics. The hemodynamic forces represent the integral of blood flow momentum over the LV volume. We normalized the instantaneous value of the hemodynamic force with the corresponding value of LV volume, to facilitate comparison between patients with different LV size. It was then divided by the fluid density and gravity acceleration to have a dimensionless number corresponding to the force expressed as a percentage of gravity acceleration (or of the static weight of the same volume of blood). The normalized force represented the average value of the pressure gradient in the LV cavity (up to a multiplicative constant that depends on the chosen dimensional units). The longitudinal hemodynamic force's time-profile was used to extract a few characteristic parameters that characterize the various phases of the cardiac cycle. Concerning Fig. 3, that displays the different phases on a typical time profile, we calculated the following parameters:

- LV longitudinal force (LVLF) as the mean amplitude of the longitudinal force throughout the cardiac cycle; since it includes both positive and negative values, the amplitude was computed as the root mean square of all values;
- LV systolic longitudinal force (LVsysLF), calculated as the LVLF above but limited to the systolic phase only;
- LV impulse (LVim) as the mean longitudinal force during the systolic propulsive phase, when the force is positive (directed from the LV cavity toward aorta); it is the area under the curve of the positive force profile during systole, normalized by the corresponding time interval;
- LV suction (LVs) as the mean longitudinal force during the period following propulsion while the force is nega-

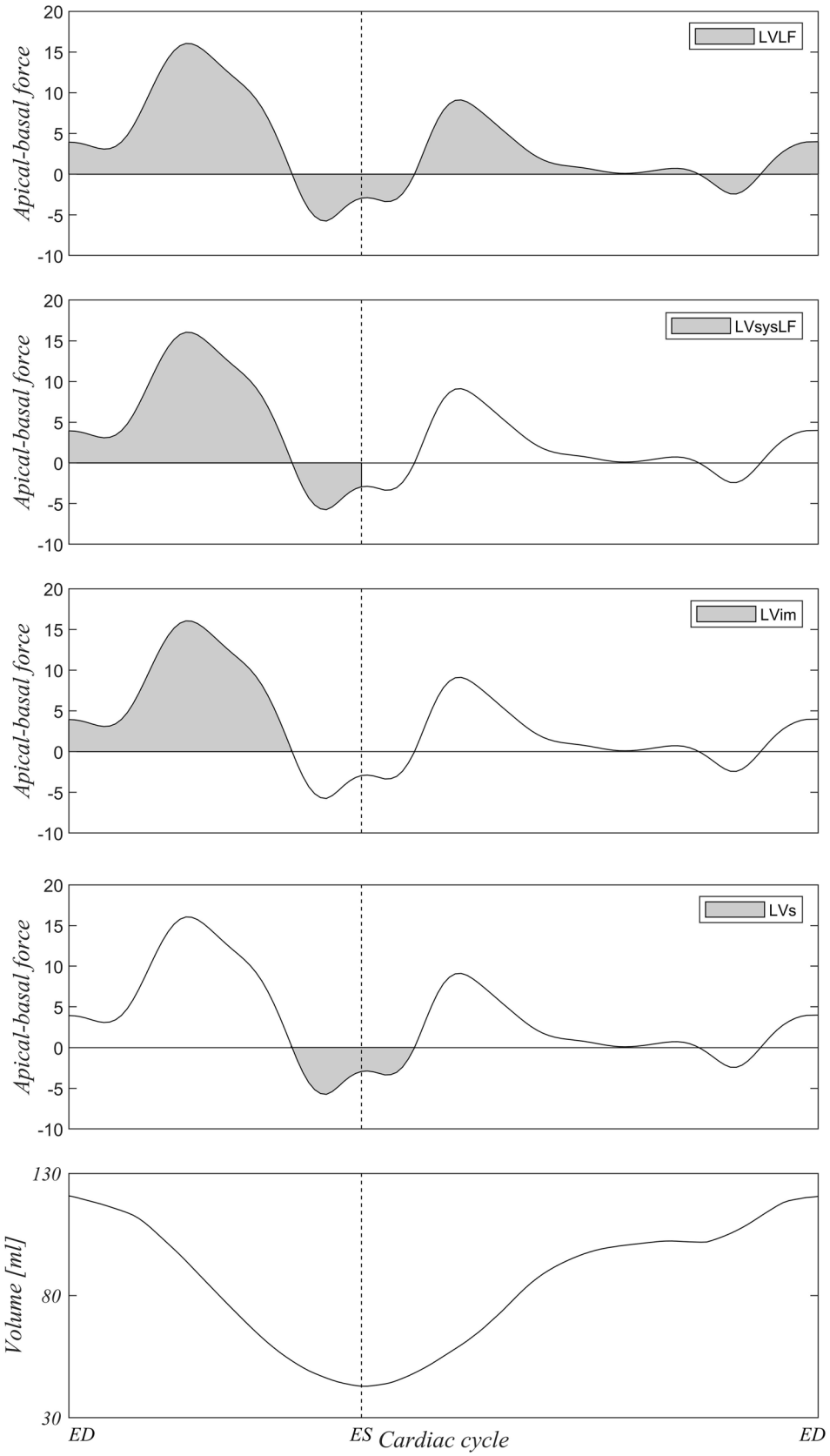

Fig. 3 Description of intervals used in the calculation of hemodynamic force parameters

tive; which is computed as the LVim but in the period comprising the end of systole (when the force decelerates the exiting flow, with Aorta open and mitral valve closed) and the initial part of diastole (the effective suction when the mitral inflow accelerates, with Aorta closed and mitral valve open);

The calculation of the parameters of the hemodynamic force was performed with a prototype software (2DCPA v.1.4; TomTec Imaging Systems Gmbh, Unterschleissheim, Germany) that is identical to the version used for strain and volumes with the only difference of the additional capability of The calculation of the parameters of the hemodynamic force was performed quantification.

Statistical analysis

Continuous variables were expressed as means ± standard deviation (SD). We divided the study population into three age groups: 16–39 years, 40–59 years, > 60 years. Differences between groups were analyzed for statistical significance using Student's t-test for continuous variables, the chi-square test and Fisher's exact test for categorical variables. Through the linear regression analysis, we calculated the correlations between continuous variables. Intra-observer and inter-observer variability were assessed in 10 randomly selected subjects by calculating the intra-class correlation coefficient (ICC) and 95% confidence intervals (CIs) of the LV strain components and volumes. Statistical tests were performed using SPSS version 22 (IBM, Armonk, New York) and MatLab (Natick, MA, USA; R2019b). The null hypothesis was rejected for $P < 0.05$.

Results

Clinical and echocardiographic data and gender differences

The final study population included 176 subjects (87 men and 89 women, mean age 47 ± 18 years, age range 16–82) divided into three age groups. Demographic data and echocardiographic parameters are reported in Table 1. All the subjects presented standard LV geometry, cardiac mass, EF, and the males had a higher LV mass index and larger LV volumes ($p < 0.0001$). LV diastolic function grade I was found in twelve patients (7%) according to the ASE/EACVI criteria, whereas no subjects had Grade II or III of diastolic dysfunction. By gender-specific analysis, no differences were detected between the mean values of longitudinal strain and myocardial GCS, except that women showed a slight increased endocardial GCS ($p = 0.05$). The calculation of the parameters of hemodynamic forces was performed, resulting higher in men than in women ($p < 0.0001$) except for LVs (p = ns).

Age and parameters of cardiac mechanics

Table 2 reports the average value of the volumetric, deformation, and hemodynamic force's parameters for the different age groups separated by gender. LV volumes decrease significantly in patients over 60 years of age in both men and women ($p < 0.0001$ with both younger groups). LVEF slightly rises in the same subgroup of patients ($p < 0.0001$) as well as LV mass indexed to BSA ($p = 0.002$). The continuous variation of these parameters with age is shown in Fig. 4. Both EDV and ESV present a significant decrease with age ($r = 0.37$ and $r = 0.38$, respectively), while LVEF and LV mass indexed to BSA show an increase ($r = 0.28$ for both). The variations of global strain are shown in Fig. 5. Myocardial and endocardial GCS values improve with age ($r = 0.33$ and $r = 0.31$, respectively) with statistically significant differences among all the groups. On the opposite, myocardial and endocardial GLS decline with age ($r = 0.38$ and $r = 0.45$, respectively), with statistically significant differences in the older group. The correlation coefficients with age of all these echocardiographic parameters mentioned above are overall low, as age alone is not expected to be predictive and only exhibit a tendency; nevertheless, results present a statistical significance. The longitudinal and circumferential deformation values measured at the endocardial regions are higher than those over the myocardial thickness ($p < 0.0001$, data not shown in table). We also verified the relationship reported above between LVEF, endocardial GLS, and GCS; the correlation coefficient of the identity LVEF model = LVEF was equal to $r = 0.96$. The time profile of the longitudinal hemodynamic forces averaged over the entire population (with shaded variability ± SD) is shown in Fig. 6. All profiles presented a consistent shape over the entire average l population, characterized by a positive systolic (propulsive) peak, followed by a negative value in the transition from systole to diastole. All hemodynamic force's parameters decrease with age, except for LVs, Fig. 7. This behavior is more marked for the systolic parameters (LVsysLF, $r = 0.30$; LVim $r = 0.36$), and it is weaker for the overall cycle (LVLF, $r = 0.2$). For the same parameters, the eldest group presents a statistically significant decrease in both younger groups.

Table 1 Demographic data and echocardiographic parameters. Data are expressed as mean ± SD or percentages

Variables	Men 87 pts (mean ± SD)	Women 89 pts (mean ± SD)	Total population 176 pts (mean ± SD)	*P**
Age (years)	42 ± 17	47 ± 17	47 ± 18	ns
Body mass index (kg/m^2)	24 ± 3	24 ± 5	24 ± 2	ns
Body surface area (m^2)	1.95 ± 0.16	1.74 ± 0.19	1.85 ± 0.2	< 0.0001
Heart rate (beats/minute)	68 ± 11	72 ± 10	70 ± 11	0.02
Systolic blood pressure (mmHg)	131 ± 17	126 ± 19	128 ± 18	ns
Diastolic blood pressure (mmHg)	75 ± 11	77 ± 12	76 ± 11	ns
LV EDV (ml)	127 ± 28	85 ± 18	106 ± 31	< 0.0001
LV ESV (ml)	47 ± 12	31 ± 8	39 ± 13	< 0.0001
LV mass index (g/m^2)	85 ± 17	74 ± 15	80 ± 17	< 0.0001
LV ejection fraction (%)	62 ± 7	63 ± 4	62 ± 6	ns
RWT	0.35 ± 0.06	0.36 ± 0.05	0.36 ± 0.05	ns
Peak S′ (cm/s)	9.4 ± 1.8	8.4 ± 2.0	8.9 ± 2.1	0.002
E wave of transmitral flow (cm/sec)	79.3 ± 19.5	80.9 ± 16.8	80.1 ± 18.2	ns
A wave of transmitral flow (cm/sec)	58.0 ± 18.3	67.5 ± 20.8	62.6 ± 20.1	0.003
E/A	1.4 ± 0.5	1.3 ± 0.5	1.4 ± 0.5	ns
E/E′	7.1 ± 2.3	8.4 ± 3.2	7.7 ± 2.8	0.004
Myocardial GLS (%)	− 21.9 ± 2.2	− 21.3 ± 2.3	− 21.6 ± 2.2	ns
Endocardial GLS (%)	− 24.2 ± 2.6	− 23.9 ± 2.8	− 24.0 ± 2.7	ns
Myocardial GCS (%)	− 24.1 ± 3.5	− 24.4 ± 2.6	− 24.2 ± 3.1	ns
Endocardial GCS (%)	− 30.6 ± 4.2	− 31.8 ± 3.7	− 31.3 ± 4.0	0.05
LVLF (%)	16.2 ± 5.3	13.2 ± 3.6	14.8 ± 4.8	< 0.0001
LVsysLF (%)	25.1 ± 7.9	19.4 ± 5.6	22.4 ± 7.4	< 0.0001
LVIm (%)	20.4 ± 7	16.6 ± 5.2	18.7 ± 6.5	< 0.0001
LVs (%)	8.8 ± 2.4	8.1 ± 2.4	8.5 ± 2.4	ns

EDV end diastolic volume, *ESV* end systolic volume, *GCS* global circumferential strain, *GLS* global longitudinal strain, *LV* left ventricle, *LVIm* left ventricle impulse, *LVLF* LV longitudinal force, *LVs* left ventricle suction, *LVsysLF* left ventricle systolic longitudinal force, *Peak E'* early diastolic Tissue Doppler velocity of mitral annulus, *Peak S'* systolic peak Tissue Doppler velocity of mitral annulus, *RWT* relative wall thickness

*P-value differences between gender

Reproducibility

Reproducibility analyses performed on the same set of images in 20 subjects are summarized in Table 3. Intra-observer and inter-observer analysis showed excellent repeatability and reproducibility. Intra-class correlation varies between 0.944 and 0.991 ($p < 0.01$) on three intra-observers evaluations for both strain components, and it is 0.965 and 0.978 ($p < 0.01$) in inter-observer analysis with a linear correlation coefficient equal to 0.96 for each. This analysis also demonstrated that LVLF present a reproducibility comparable to that of strain and volumetric measurement.

Discussion

We presented a prospective study in which normality values are established through an integrated approach to cardiac mechanics in a large cohort of healthy volunteers and over a wide range of ages. We demonstrated that: (a) after aging, the systolic components of hemodynamic forces decline uniformly; (b) the LV mass mildly increases despite being still in the normal range; (c) the LV volumes decrease; (d) the values of GLS and GCS behave oppositely, the former gradually decreases while the latter increases and (e) there is a slight improvement in LVEF

Table 2 Echocardiographic parameters according to age; Data are expressed as mean ± SD or percentages

	Age 16–39 (Group 1) (n = 57 pts)		Age 40–59 (Group 2) (n = 64 pts)		Age ≥ 60 (Group 3) (n = 55 pts)		*P** Patient 's groups		
	Male mean ± SD	Female mean ± SD	Male mean ± SD	Female mean ± SD	Male mean ± SD	Female Mean ± SD	1 vs 2	2 vs 3	1 vs 3
LVEDV (ml)	145 ± 18	85 ± 18	125 ± 25	96 ± 22	109 ± 32	82 ± 16	ns	< 0.0001	< 0.0001
LVESV (ml)	55 ± 8	32 ± 9	47 ± 10	34 ± 11	39 ± 13	29 ± 7	ns	< 0.0001	< 0.0001
LVEF (%)	62 ± 3	63 ± 4	63 ± 4	64 ± 5	64 ± 4	65 ± 3	ns	0.01	< 0.0001
LVMi (g/m^2)	82 ± 13	66 ± 12	86 ± 17	74 ± 19	97 ± 16	79 ± 15	ns	ns	0.002
Myo-GLS (%)	− 22.2 ± 2.1	− 22.2 ± 2.4	− 21.9 ± 2.4	− 21.4 ± 1.9	− 19.3 ± 1.3	− 19.8 ± 1.2	ns	< 0.0001	< 0.0001
Endo-GLS (%)	− 24.7 ± 2.1	− 24.7 ± 2.7	− 24.1 ± 2.9	− 24.3 ± 2.5	− 21.5 ± 1.2	− 21.9 ± 1.4	ns	< 0.0001	< 0.0001
Myo-GCS (%)	− 22.6 ± 3.3	− 23.3 ± 2.7	− 24.2 ± 3.3	− 24.4 ± 3.0	− 26.5 ± 2.3	− 25.1 ± 2.9	0.01	0.03	< 0.0001
Endo-GCS (%)	− 28.9 ± 3.4	− 30.3 ± 3.7	− 30.6 ± 4.0	− 32.1 ± 4.3	− 34.6 ± 3.0	− 32.3 ± 4.4	0.01	0.04	< 0.0001
LVLF (%)	16.6 ± 4.3	13.5 ± 3.6	17.1 ± 6.7	14.6 ± 3.8	14.3 ± 3.8	12 ± 3.2	ns	< 0.0001	0.002
LVsysLF (%)	27.9 ± 6.6	19.3 ± 5.1	25.4 ± 9	21.8 ± 6.1	20.1 ± 5.6	17.7 ± 5	ns	< 0.0001	< 0.0001
LVIm (%)	23.9 ± 5.6	16.5 ± 4.8	20.1 ± 8	18.8 ± 5.9	16.1 ± 4.5	15.2 ± 4.5	ns	< 0.0001	< 0.0001
LVs (%)	8.3 ± 2.1	8.6 ± 2.4	9 ± 2.6	7.7 ± 2.6	9.3 ± 2.3	8.1 ± 2.3	ns	ns	ns

SD standard deviation, *LV* left ventricle, *LVMi* left ventricle mass indexed to body surface area, *Myo-GLS* myocardial global longitudinal strain, *Endo-GLS* endocardial global longitudinal strain, *Myo-GCS* myocardial global circumferential strain, *Endo-GCS* endocardial global longitudinal strain, *LVIm* left ventricle impulse, *LVLF* left ventricle longitudinal force, *LVs* left ventricle suction, *LVsysLF* left ventricle systolic longitudinal force

*P-value differences between age groups

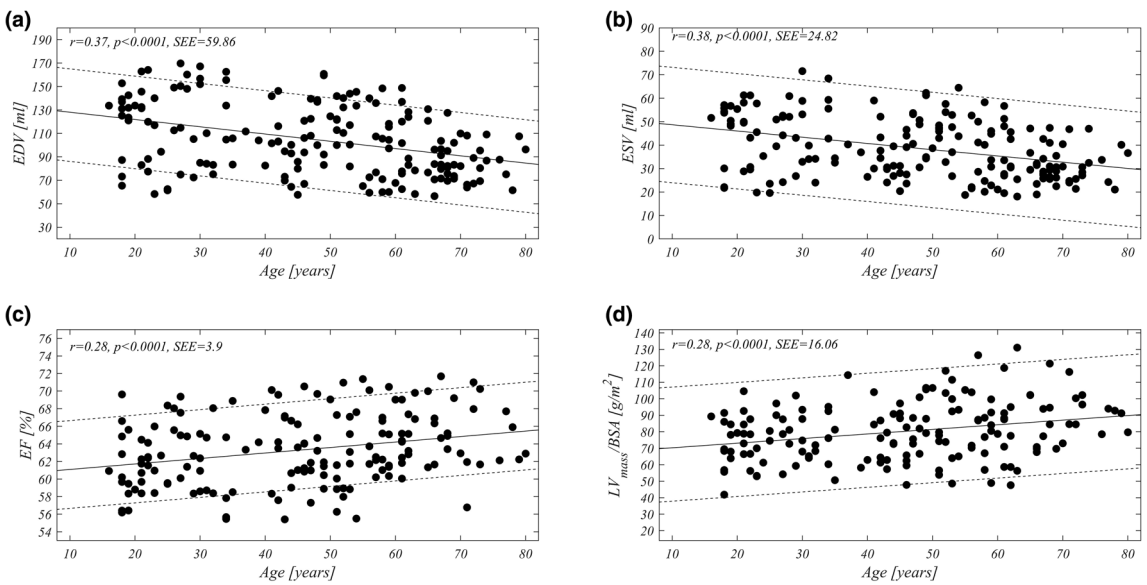

Fig. 4 Relations of age (horizontal axis) with (vertical axes): **a** LV end-diastolic volume (EDV), **b** end-systolic volume (ESV), **c** ejection fraction (EF) and **d** LV mass indexed to BSA. Solid dots represent the study population with fitted regression line (continuous line) and 5th–95th percentile prediction bands (parallel dotted lines). *SEE* standard error estimate

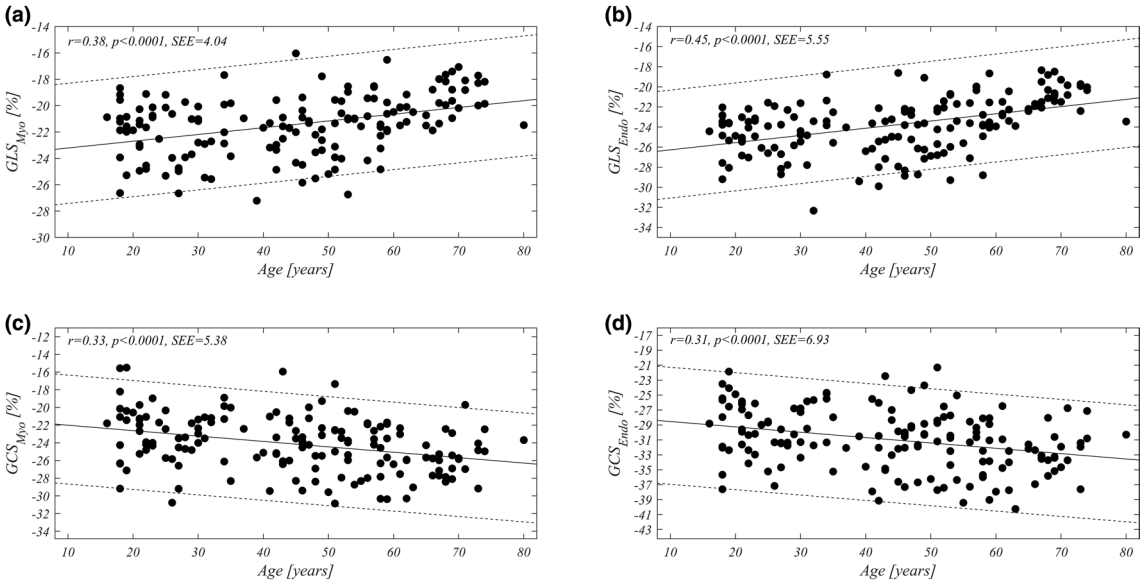

Fig. 5 Relations of age (horizontal axis) with (vertical axes): **a** myocardial GLS, **b** endocardial GLS, **c** myocardial GCS, **d** endocardial GCS. Solid dots represent the study population with fitted regression line (continuous line) and 5th–95th percentile prediction bands (parallel dotted lines). *SEE* standard error estimate

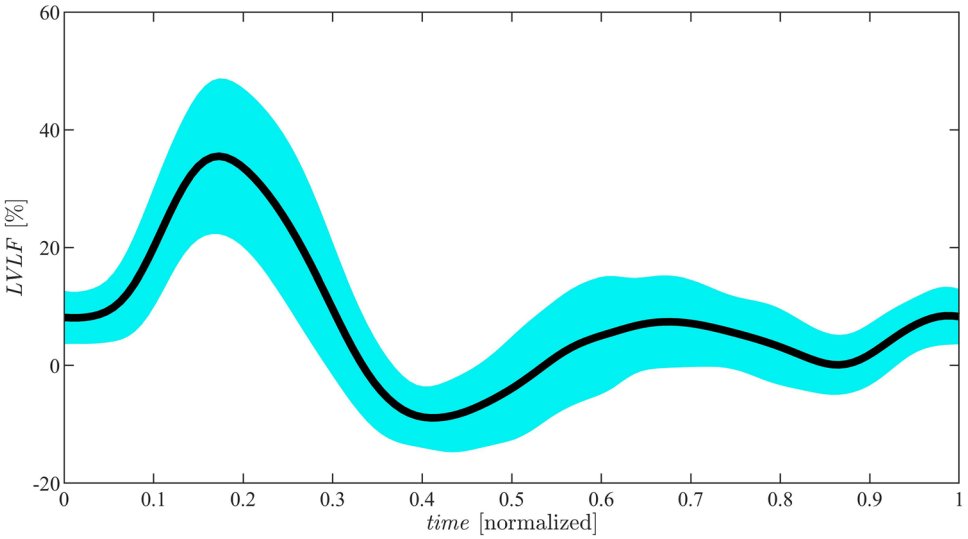

Fig. 6 Time profile of the longitudinal hemodynamic force averaged over the entire population; the shade indicates ± SD interval

after these processes. For the calculation of both longitudinal and especially circumferential strain, we used software to analyze the images from the three apical views. The new system has allowed overcoming the known limits due to the deformation artifacts deriving from through-plane displacements in the short axis views [17, 20]. Consistent with previous studies of cardiac magnetic resonance (CMR) and echocardiography [21], overall endocardial strain values resulted higher than those of the myocardium due to higher metabolic rates, oxygen extraction, and coronary flow of the endocardium [22]. As described in 2D and 3D echocardiographic studies, the circumferential

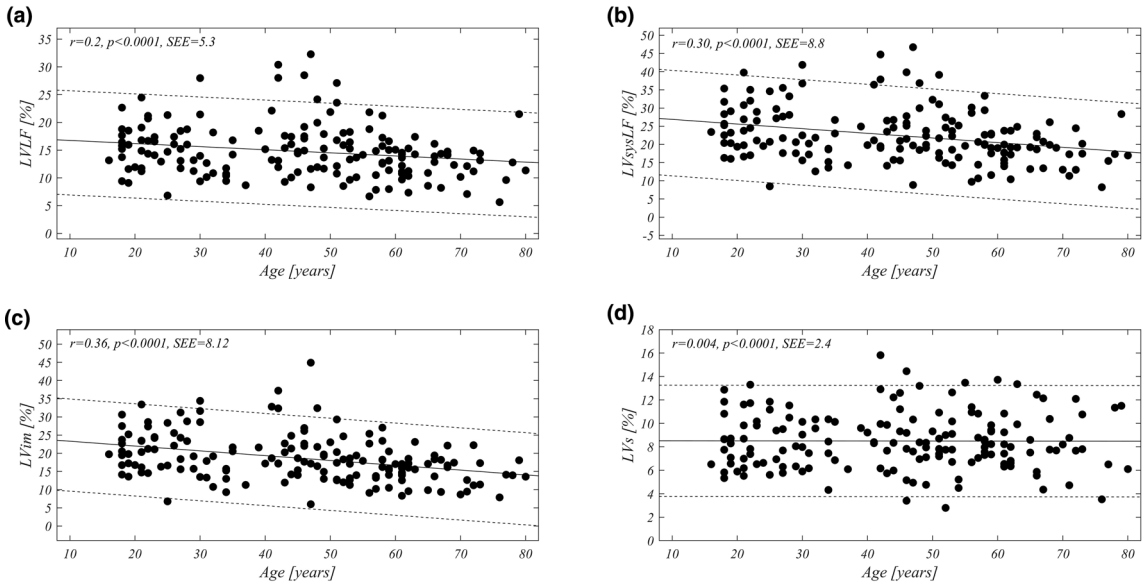

Fig. 7 Relations of age (horizontal axis) with (vertical axes): **a** LV longitudinal force (LVLF), **b** LV systolic longitudinal force (LVsysLF), **c** LV longitudinal force impulse (LVim), **d** LV longitudinal force suction (LVs). Solid dots represent the study population with fitted regression line (continuous line) and 5th–95th percentile prediction bands (parallel dotted lines). *SEE* standard error estimate

strain increases progressively with aging [20, 23]; conversely, data relating to GLS are controversial. Marwick et al. showed that GLS did not decrease over time [24] while in the NORRE multicenter study, GLS was higher in women, and there was no relationship with the age; however, patients over 60 years were less numerous [25]. More recently, Galderisi et al. clearly showed that the decline of GLS is significant in the decades 50–60 and over 60 [23], and this result was also confirmed by Muraru et al. in a 3D echo population [20]. It is widely accepted that age-related changes in cardiovascular structure and function occur in healthy subjects. In our study population, we observed that the decline in longitudinal strain depended on the age and was linked to further pathophysiological changes: the compensatory increase in circumferential strain and LV mass without reaching LV hypertrophy values, the decrease in the LV volumes and finally the compensatory increase in LVEF to maintain cardiac output. These data are in line with previous studies where dedicated software from different vendors was used [26] or such as the MESA study, where CMR was used to examine age-related differences in the structure and function of LV [27].

Relationship between deformation imaging and LVEF

Longitudinal and circumferential strain actively contributes to the LV volumetric reduction during the systole and so to the ejection fraction. We recently provided a mathematical model relating to LVEF and strain [4, 8]. Our study population found an excellent correlation coefficient between the LVEF model and the LVEF calculated with the Simpson method.. This relationship between the "deformation plane" described by GLS (x coordinate), GCS (y coordinate), and the curves at constant LVEF is graphically described in Fig. 8. This graphical representation shows that the same LVEF can be obtained with different pairs of GLS and GCS corresponding to different points along the corresponding curve [4]. In this graph, the present population is distributed within a limited region corresponding to normal contraction values. However, it shows that aging is associated with a tendency to displace along the lower-right direction, which corresponds to a decrease of GLS accompanied to a compensatory increase of GCS to ensure the preservation or a weak increased LVEF. This attempt of integration between LVEF and deformation imaging should facilitate the interdependent use of these parameters, going beyond the conventional

Table 3 Intra-observer and inter-observer variability between the three operators

Variables	Intra-class correlation (rho)	95% Confidence Intervals	*P**
Intra-observer variability 1			
Endocardial GLS	0.988	0.951–0.997	< 0.01
Endocardial GCS	0.991	0.962–0.998	< 0.01
LVLF	0.997	0.994–0.998	< 0.01
EDV	0.959	0.833–0.990	< 0.01
ESV	0.981	0.922–0.995	< 0.01
Intra-observer variability 2			
Endocardial GLS	0.960	0.868–0.981	< 0.01
Endocardial GCS	0.944	0.877–0.993	< 0.01
LVLF	0.915	0.971–0.991	< 0.01
EDV	0.968	0.927–0.996	< 0.01
ESV	0.924	0.942–0.989	< 0.01
Intra-observer variability 3			
Endocardial GLS	0.945	0.742–0.988	< 0.01
Endocardial GCS	0.971	0.938–0.977	< 0.01
LVLF	0.972	0.957–0.988	< 0.01
EDV	0.993	0.978–0.995	< 0.01
ESV	0.988	0.933–0.992	< 0.01
Inter-observer variability			
Endocardial GLS	0.965	0.937–0.996	< 0.01
Endocardial GCS	0.978	0.972–0.992	< 0.01
LVLF	0.991	0.988–0.993	< 0.01
EDV	0.957	0.933–0.991	< 0.01
ESV	0.961	0.923–0.995	< 0.01

EDV end diastolic volume, *ESV* end systolic volume, *GCS* global circumferential strain, *GLS* global longitudinal strain, *LVLF* Left ventricle longitudinal force

limit of individual and one-dimensional use of these values [28, 29]. This approach could quickly identify both a subtle and progressive deterioration of the LV mechanical function and an improvement of the same, thanks to the shifts from the normal region.

Reference values for LV hemodynamic forces

This study is the first to apply an extension of the strain software package for echocardiography dedicated to the determination of reference values and normal limits of hemodynamic force's parameters for a relatively large cohort of healthy subjects. The values are consistent with previous results obtained in smaller groups of healthy subjects with 4D Flow MRI [30] (consider that hemodynamic forces expressed in % should be divided by 10 to be transformed in N/l) and with cine cardiac MRI [5]. These normality values provide first landmarks for future studies, including this innovative property of LV function in pathological cohorts. We identified significant age and gender differences in hemodynamic force's parameters: in men, they were higher than in women, probably due to higher LV masses indexed with BSA. After the age of 40, HDF follows the fate of GLS and progressively decreases. The apparent paradox of mildly increased LVEF associated with the falling parameters of the longitudinal function and the GLS seems justified by reducing the ventricular volumes and the progressive improvement of the circumferential function. In this scenario, LVs represents the only parameter that is not influenced by age or gender.

Limitations

This study presents several limitations. First, this is a single-center, single-ethnicity study. The relatively small sample size of our Caucasian population cannot be generalized to the entire population. However, the rigorous methodology in selecting healthy subjects and analyzing images represents a considerable effort and a reasonable sample in a single center. Second, we did not validate the accuracy of strain measurements against reference standards such as CMR in our subjects. Third, we did not compare the value of GLS and GCS between the different ultrasound vendors. Inter-vendor variability exists even in full-thickness strain due to the differences in the analytical algorithm. Forth, the apical approach to GCS could be less accurate for either the limited lateral resolution of ultrasound images or because the entire circumference is not visible from the apical views. The former was shown not to be critical in a comparative study [17], the latter is minimized by using a triplane evaluation, reducing artifacts in deformation such as those that may result from through-plane displacements of 3D geometry. Lastly, the current approach should be considered an estimation of hemodynamic forces since the analysis is dependent on 2D image quality and frame rates.

Conclusion

The GLS and GCS are progressively and firmly entering daily clinical practice; moreover, the flow force's quantifications promise a further level of knowledge of the LV fun ction. This integrated approach could help differentiate normality from pathology; however, it needs extensive validation in further clinical studies before being accepted into clinical practice.

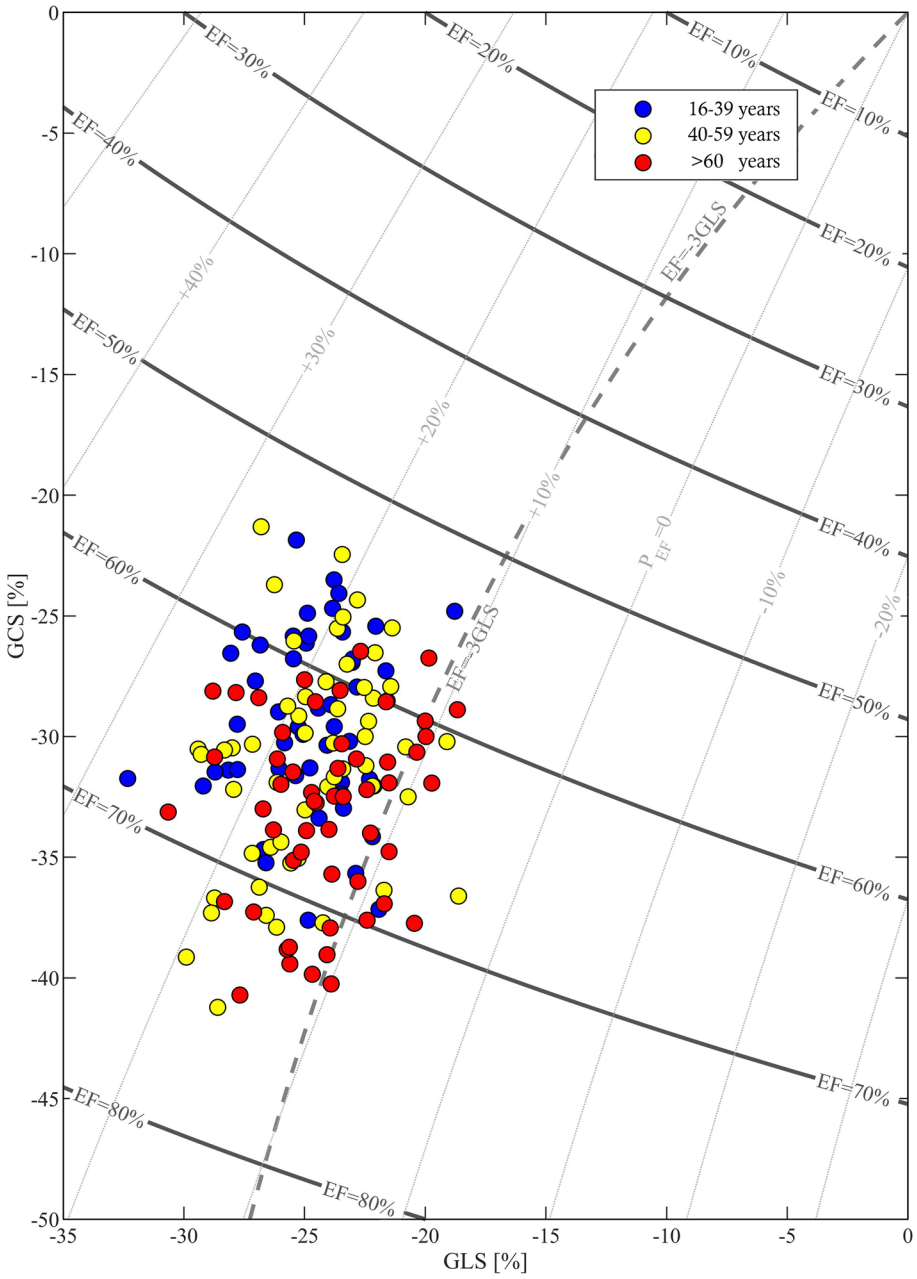

Fig. 8 "Deformation plane" with strain properties of the study population. Curved bands in the GLS-GCS plane represent the regions with constant value of EF. Patients aged > 60 years, present a conserved or slightly increased EF with respect to the other younger groups, thus they tend to displace on the right along the curves of constant EF, which correspond to a reduction of GLS and slight increase of GCS

Author contributions GF and GP conceived and designed research; GF, GP and DC interpreted results of experiments; DC prepared figures; DC, and GP analyzed data; SF, LP, MZ, performed experiments; GF, and GP drafted manuscript; ADL edited and revised manuscript; GF, DC, SF, LP, MZ, GP, and ADL approved final version of manuscript.

Funding DC and GP received partial support for this study from the Italian Ministry of Education and Research, project PRIN No. 2017A889FP.

Compliance with ethical standards

Conflict of interest GP is s senior scientific consultant for Medis Medical Imaging Systems BV (Leiden, The Netherlands). GF, DC, SF, LP, MZ and ADL have no conflict of interest to declare.

References

1. Solomon SD, Anavekar N, Skali H, McMurray J, Swedberg K, Yusuf S et al (2005) Influence of ejection fraction on cardiovascular outcomes in a broad spectrum of heart failure patients. Circulation 112(24):3738–3744
2. Tops LF, Delgado V, Marsan NA, Bax JJ (2017) Myocardial strain to detect subtle left ventricular systolic dysfunction. Eur J Heart Fail 19(3):307–313
3. Knuuti J, Wijns W, Saraste A, Capodanno D, Barbato E, Funck-Brentano C et al (2020) 2019 ESC Guidelines for the diagnosis and management of chronic coronary syndromes. Eur Heart J 41:407–477
4. Pedrizzetti G, Lapinskas T, Tonti G, Stoiber L, Zaliunas R, Gebker R et al (2019) The Relationship Between EF and Strain Permits a

More Accurate Assessment of LV Systolic Function. J Am Coll Cardiol Img 12(9):1893–1895
5. Lapinskas T, Pedrizzetti G, Stoiber L, Düngen HD, Edelmann F, Pieske B et al (2019) The intraventricular hemodynamic forces estimated using routine CMR cine images: a new marker of the failing heart. J Am Coll Cardiol Imaging 12(2):377–379
6. Arvidsson PM, Töger J, Carlsson M, Steding-Ehrenborg K, Pedrizzetti G, Heiberg E et al (2017) Left and right ventricular hemodynamic forces in healthy volunteers and elite athletes assessed with 4D flow magnetic resonance imaging. Am J Physiol 312:H314–H328
7. Eriksson J, Bolger AF, Ebbers T, Carlhäll CJ (2016) Assessment of left ventricular hemodynamic forces in healthy subjects and patients with dilated cardiomyopathy using 4D flow MRI. Physiol Rep 4:741–747
8. Dal Ferro M, Stolfo D, De Paris V, Lesizza P, Korcova R, Collia D et al (2018) Cardiac fluid dynamics meets deformation imaging. Cardiovasc Ultrasound 16(1):1–10
9. Cosyns B, Garbi M, Separovic J, Pasquet A, Lancellotti P (2013) Update of the Echocardiography Core Syllabus of the European Association of Cardiovascular Imaging (EACVI). Eur Heart J Cardiovasc Imaging 14(9):837–839
10. Lang RM, Badano LP, Mor-Avi V, Afilalo J, Armstrong A, Ernande L et al (2015) Recommendations for cardiac chamber quantification by echocardiography in adults: an update from the American society of echocardiography and the European association of cardiovascular imaging. Eur Heart J Cardiovasc Imaging 16(3):233–271
11. Devereux RB, Alonso DR, Lutas EM, Gottlieb GJ, Campo E, Sachs IRN (1986) Echocardiographic assessment of left ventricular hypertrophy: comparison to necropsy findings. Am J Cardiol 57:450–458
12. Lang RM, Bierig M, Devereux RB, Flachskampf FF, Foster E, Pellikka PA et al (2005) Recommendations for chamber quantification: a report from the American Society of Echocardiography's guidelines and standards committee and the Chamber Quantification Writing Group, developed in conjunction with the European Association of Echocardiograph. J Am Soc Echocardiogr 18(12):1440–1463
13. Nagueh SF, Smiseth OA, Appleton CP, Byrd BF, Dokainish H, Edvardsen T et al (2016) Recommendations for the evaluation of left ventricular diastolic function by echocardiography: an update from the American Society of Echocardiography and the European Association of Cardiovascular Imaging. Eur Heart J Cardiovasc Imaging 17(12):1321–1360 **Epub 2016 Jul 15**
14. Voigt JU, Pedrizzetti G, Lysyansky P, Marwick TH, Houle H, Baumann R et al (2015) Definitions for a common standard for 2D speckle tracking echocardiography: consensus document of the EACVI/ASE/Industry Task Force to standardize deformation imaging. Eur Heart J Cardiovasc Imaging 16(1):1–11
15. Saito K, Okura H, Watanabe N, Hayashida A, Obase K, Imai K et al (2009) Comprehensive evaluation of left ventricular strain using speckle tracking echocardiography in normal adults: comparison of three-dimensional and two-dimensional approaches. J Am Soc Echocardiogr 22(9):1025–1030
16. Stokke TM, Hasselberg NE, Smedsrud MK, Sarvari SI, Haugaa KH, Smiseth OA et al (2017) Geometry as a confounder when assessing ventricular systolic function: comparison between ejection fraction and strain. J Am Coll Cardiol 70(8):942–954
17. Pedrizzetti G, Tanacli R, Lapinskas T, Zovatto L, Pieske B, Tonti G et al (2019) Integration between volumetric change and strain for describing the global mechanical function of the left ventricle. Med Eng Phys 74:65–72
18. Pedrizzetti G, Arvidsson PM, Töger J, Borgquist R, Domenichini F, Arheden H et al (2017) On estimating intraventricular hemodynamic forces from endocardial dynamics: a comparative study with 4D flow MRI. J Biomech 60:203–210
19. Pedrizzetti G (2019) On the computation of hemodynamic forces in the heart chambers. J Biomech 95:109323
20. Muraru D, Cucchini U, Mihăilă S, Miglioranza MH, Aruta P, Cavalli G et al (2014) Left ventricular myocardial strain by three-dimensional speckle-tracking echocardiography in healthy subjects: reference values and analysis of their physiologic and technical determinants. J Am Soc Echocardiogr 27(8):858–872
21. Altiok E, Neizel M, Tiemann S, Krass V, Kuhr K, Becker M et al (2012) Quantitative analysis of endocardial and epicardial left ventricular myocardial deformation—comparison of strain-encoded cardiac magnetic resonance imaging with two-dimensional speckle-tracking echocardiography. J Am Soc Echocardiogr 25(11):1179–1188
22. Path G, Robitaille PM, Merkle H, Tristani M, Zhang J, Garwood M et al (1990) Correlation between transmural high energy phosphate levels and myocardial blood flow in the presence of graded coronary stenosis. Circ Res 67(3):660–673
23. Alcidi GM, Esposito R, Evola V, Santoro C, Lembo M, Sorrentino R et al (2018) Normal reference values of multilayer longitudinal strain according to age decades in a healthy population: a single-centre experience. Eur Heart J Cardiovasc Imaging 19(12):1390–1396
24. Marwick TH, Leano RL, Brown J, Sun JP, Hoffmann R, Lysyansky P et al (2009) Myocardial strain measurement with 2-dimensional speckle-tracking echocardiography. Definition of normal range. J Am Coll Cardiol Imaging 2(1):80–84
25. Sugimoto T, Dulgheru R, Bernard A, Ilardi F, Contu L, Addetia K et al (2017) Echocardiographic reference ranges for normal left ventricular 2D strain: results from the EACVI NORRE study. Eur Heart J Cardiovasc Imaging 18(8):833–840
26. Coiro S, Huttin O, Bozec E, Selton-Suty C, Lamiral Z, Carluccio E et al (2017) Reproducibility of echocardiographic assessment of 2D-derived longitudinal strain parameters in a population-based study (The STANISLAS Cohort Study). Int J Cardiovasc Imaging 33(9):1361–1369
27. Cheng S, Fernandes VRS, Bluemke DA, McClelland RL, Kronmal RA, Lima JAC (2009) Age-related left ventricular remodeling and associated risk for cardiovascular outcomes the multi-ethnic study of atherosclerosis. Circ Cardiovasc Imaging 2(3):191–198
28. Potter E, Marwick TH (2018) Assessment of left ventricular function by echocardiography: the case for routinely adding global longitudinal strain to ejection fraction. J Am Coll Cardiol Img. 11(2P1):260–274
29. Tanaka H (2019) Utility of strain imaging in conjunction with heart failure stage classification for heart failure patient management. J Echocardiogr 17(1):17–24
30. Arvidsson PM, Töger J, Carlsson M, Steding-Ehrenborg K, Pedrizzetti G, Heiberg E et al (2017) Left and right ventricular hemodynamic forces in healthy volunteers and elite athletes assessed with 4D flow magnetic resonance imaging. Am J Physiol Heart Circ Physiol 312(2):H314–H328